Metal–Support Interactions

DOI: 10.1002/anie.201309248

Electronic Metal–Support Interactions in Single-Atom Catalysts**

*Pingping Hu, Zhiwei Huang, Zakariae Amghouz, Michiel Makkee, Fei Xu, Freek Kapteijn, Alla Dikhtiarenko, Yaxin Chen, Xiao Gu, and Xingfu Tang**

Abstract: *The synthesis of single-atom catalysts and the control of the electronic properties of catalytic sites to arrive at superior catalysts is a major challenge in heterogeneous catalysis. A stable supported single-atom silver catalyst with a controllable electronic state was obtained by anti-Ostwald ripening. An electronic perturbation of the catalytic sites that is induced by a subtle change in the structure of the support has a strong influence on the intrinsic reactivity. The higher depletion of the 4d electronic state of the silver atoms causes stronger electronic metal–support interactions, which leads to easier reducibility and higher catalytic activity. These results may improve our understanding of the nature of electronic metal–support interactions and lead to structure–activity correlations.*

Since the concept of strong metal–support interactions (SMSI) was first introduced to heterogeneous catalysis in 1978,[1] a thorough understanding of the nature of the SMSI effect has been lacking, although enormous efforts have been devoted to gaining an improved knowledge of the SMSI effect.[2–6] One of the early hypotheses for this effect is that the alteration of the charge state of the metal by electron transfer from or to a support leads to an improvement in the ability to activate reactants and thus influences the catalytic properties of the metal.[7] Experimentally, this hypothesis was confirmed by X-ray crystallography and UV photoemission spectroscopy.[8,9] Rodriguez and co-workers[9] successfully interpreted the significantly enhanced activity of platinum particles supported on ceria in water–gas shift reactions as "electronic metal–support interactions" (EMSI), a term that was recently coined by Campbell.[10] Possibly, the electronic perturbations that are due to the EMSI of supported late-transition-metal particle catalysts can be described as changes in the d-band centers (ε_d) relative to the Fermi level.[11] The desirable upshift in ε_d leads to a significant EMSI and thus to improved chemical and catalytic properties.

As the EMSI gives a more specific interpretation of the underlying causes for activity enhancements of supported metal particle catalysts than the classic SMSI, the use of the EMSI hypothesis as the electronic descriptor for metals is more exciting.[9–11] However, intrinsic metal effects, such as the electronic quantum size effect[12–14] and the structure–sensitivity geometrical effect,[15,16] should be ruled out for a complete understanding of the fundamental EMSI. However, for supported metal particle/cluster catalysts, a complete elimination of the intrinsic metal effects is particularly difficult or even impossible. A feasible method to solve the above problems is to develop a perfect catalyst with structurally fixed and spatially uniform single-atom active sites, but such an idealized catalyst is often thermally unstable because single atoms are prone to sintering under catalytic reaction conditions and even during catalyst preparation.[17,18]

Herein, to study the nature of the EMSI independent of intrinsic metal effects, two thermally stable single-atom catalysts (SAC) were designed with different d electronic states for the catalytically active sites (CAS), in which single silver atoms are firmly and uniformly anchored at the pore openings (the {001} top facets) of a microporous hollandite manganese oxide (HMO; Supporting Information, Figure S1). One SAC was synthesized from a traditional supported silver particle sample (Ag/HMO) by anti-Ostwald ripening (Ag_{AOR}–HMO).[19] The other SAC was prepared by conventional wet impregnation with $AgNO_3$ as a precursor (Ag_{IMP}–HMO). The structures and electronic states of two single-atom silver catalysts (Ag–HMO) were intensively studied to establish the EMSI and to further correlate structure and activity.

The morphology and structure of the HMO rods that grow along the $<001>$ direction and expose the {110} side facets and the {001} top facets were previously studied (Figure S2).[19–21] These features remain unchanged after the addition of the silver regardless of the preparation method, as confirmed by high-resolution transmission electron microscopy (TEM; Figure 1a,b) and TEM (Figure S3). The single silver atoms are queued in a line, which corresponds to the structure models shown in Figure S4.[22]

[*] P. Hu,[+] Z. Huang,[+] F. Xu, Y. Chen, Dr. X. Gu, Prof. X. Tang
Shanghai Key Laboratory of Atmospheric Particle Pollution and Prevention (LAP^3)
Department of Environmental Science and Engineering
Fudan University
220 Handan Road, Shanghai, 200433 (China)
E-mail: tangxf@fudan.edu.cn
Dr. Z. Amghouz[+]
Unidad de Microscopia Electrónica
Servicios-Científico Técnicos
Universidad de Oviedo-CINN
Oviedo, 33006 (Spain)
Prof. M. Makkee, Prof. F. Kapteijn, Dr. A. Dikhtiarenko
Catalysis Engineering
Department of Chemical Engineering
Delft University of Technology
2628 BL Delft (The Netherlands)
[+] These authors contributed equally to this work.

[**] This work was financially supported by the NSFC (21277032), the NCET (120131), the SCAPC (201306), and the Netherlands–China exchange program (13CDP013). The XAS and SXRD measurements were conducted at the Shanghai Synchrotron Radiation Facility, Chinese Academy of Sciences. We acknowledge Bart van der Linden and Jorrit Posthuma de Boer for their assistance with the TAP experiments.

Supporting information for this article is available on the WWW under http://dx.doi.org/10.1002/anie.201309248.

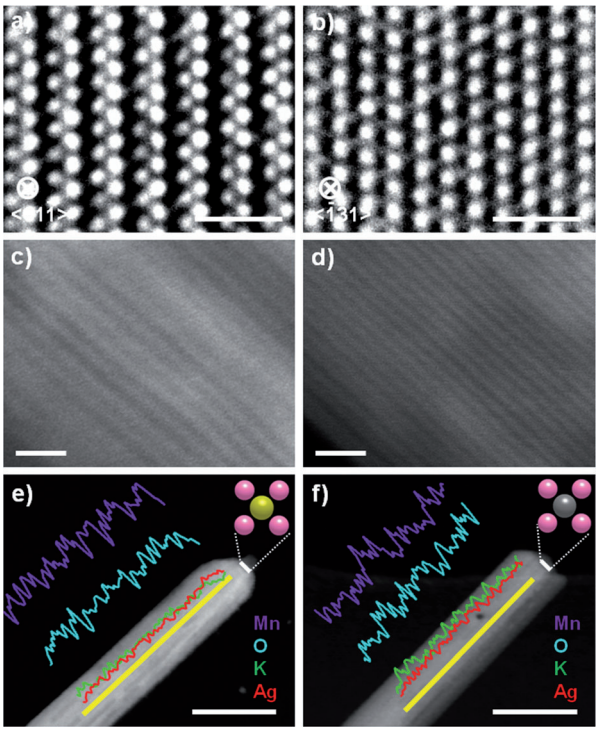

Figure 1. High-resolution TEM and HAADF-STEM images and EDX line scans along the yellow lines of Ag_{AOR}–HMO (a, c, e) and Ag_{IMP}–HMO (b, d, f). Corresponding models of the CAS on the (001) planes (e, f). Oxygen pink, silver yellow (e) or silver (f). Scale bars: 1 nm (a, b), 2 nm (c, d), 40 nm (e, f).

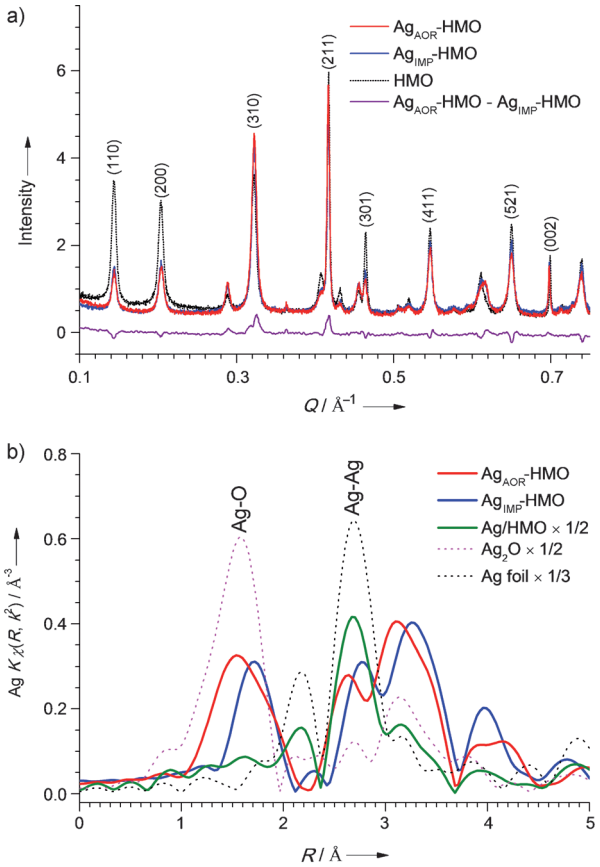

Figure 2. a) SXRD patterns and ΔSXRD pattern. b) Ag K-edge $\chi(R)$ k^2-weighted FT-EXAFS spectra of the samples.

The positions of the silver atoms in Ag–HMO were confirmed by high-angle annular dark-field scanning transmission electron microscopy (HAADF-STEM). The intensity contributed by an atom is approximately proportional to Z^2 (where Z is the atomic number).[23] High-resolution HAADF-STEM images of Ag–HMO are presented in Figure 1 c, d. The great contrast arises from the difference in atomic number between the heavier silver atoms ($Z_{Ag} = 47$) and the lighter manganese and oxygen atoms ($Z_{Mn} = 25$, $Z_O = 8$). The white lines in the $< 001 >$ orientation were clearly observed and can be ascribed to line-shaped silver atom chains in the pores of the HMO according to point and line energy-dispersive X-ray (EDX) spectroscopy (Figure 1 e, f; see also Figure S5). According to the STEM-EDX line profile analysis of the ends of the Ag–HMO rods, the forthcoming structural characterizations, and our recent report,[19] all of the silver atoms in Ag–HMO have been inserted into the pores of the HMO to expose single-atom silver sites on the {001} facets.[19] Therefore, two structural models of the single-atom CAS are shown in the insets of Figure 1 e, f, each of which is anchored at four-fold oxygen-coordinated hollow sites at the {001} pore opening of the HMO.

The subtle structural difference between the two Ag–HMO samples was determined by synchrotron X-ray powder diffraction (SXRD) and synchrotron X-ray absorption spectroscopy (XAS; Figure 2). Both the intensity and the location of the HMO reflections are distinctly modified after the addition of silver, reflecting the occupation of the HMO pores by silver atoms.[19] Although the similar reflections of the two Ag–HMO samples as a function of momentum transfer (Q) can be readily indexed to the hollandite tetragonal structure (Figure 2 a),[19,22] a subtle difference between the two Ag–HMO structures can be observed from the differential SXRD pattern (ΔSXRD) by subtracting the Ag_{IMP}–HMO pattern from that of Ag_{AOR}–HMO (Figure 2 a). Obviously, the difference can be deduced from the changes in intensity and the shifts of the reflections, which implies that the different environments of the silver atoms originate from different metal–support interactions.

The local structures of the silver atoms were determined by Fourier transform (FT) extended X-ray absorption fine structure (EXAFS) spectroscopy (Figure 2 b; see also Figure S6). The structural parameters were calculated by fitting the spectra to the corresponding models (Table S1).[22] The FT spectra of the two Ag–HMO materials are significantly different from the spectra of Ag/HMO, silver foil, and Ag_2O. The interatomic distances in the two near-neighbor shells (Ag–O and Ag–Ag) for Ag_{AOR}–HMO are slightly shorter than those of Ag_{IMP}-HMO. These results possibly reflect the interactions between silver and oxygen/silver atoms that are stronger for Ag_{AOR}–HMO than for Ag_{IMP}–HMO. The different multiple scattering features for the two Ag–HMO structures in the silver K-edge X-ray absorption near edge structure (XANES) spectra (Figure 3 a, inset) also confirm the differences in local structure.

The small structural difference between the Ag–HMO materials possibly results in the difference in the density of

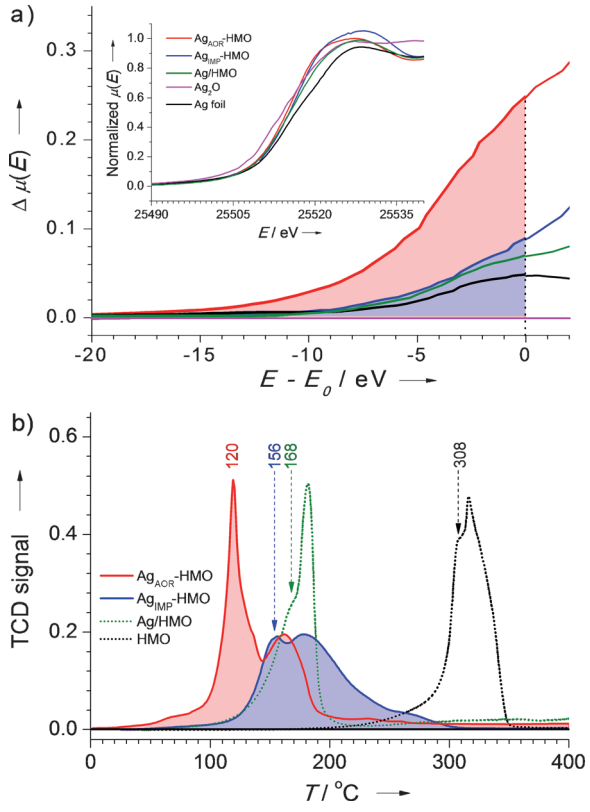

Figure 3. a) Ag K-edge XANES (inset) and ΔXANES spectra of the samples. E_0 represents the absorption threshold energy. b) Temperature-programmed H_2 reduction profiles of the samples marked with the onset reduction temperatures.

states (DOS) of the silver frontier orbitals. The Ag K-edge XANES spectra as a function of absorption energy (E) for the Ag–HMO materials are shown in the inset of Figure 3a. The "white line" of Ag_{AOR}–HMO is more intense than that of Ag_{IMP}–HMO and three reference samples, which indicates a decrease in the number of electrons in the silver frontier d-sp orbitals. The edge positions for the Ag–HMO appear between those of the silver foil and Ag_2O, indicating intermediate valence states between Ag^0 and Ag^+, which is in agreement with the X-ray photoelectron spectra (XPS; Figure S7 and Table S2).

The differential XANES (ΔXANES) spectra with respect to the Ag_2O spectrum are highly sensitive and highly accurate[24,25] for exploring the very small differences in the electronic states of the Ag–HMO structures (Figure 3a). The hybridization of the silver d-sp orbitals, especially with the oxygen p orbitals, which was corroborated by O 1s XPS (Figure S8), allowed the investigation of the unoccupied d states by Ag K-edge XANES spectroscopy.[26,27] A low intensity of the Ag–HMO in the ΔXANES spectra could be ascribed to an s→d electronic transition. As Ag_2O has an almost filled d orbital configuration (d^{10}) of Ag^+, which is due to a high d→sp charge transfer energy (ca. 5.2 eV),[28] the ΔXANES spectra of Ag–HMO with pre-edge energy absorption shoulders reflect the Ag atoms of Ag–HMO with partially vacant d orbitals,[29] which possibly originates from the upshifts of the d orbital electronic states, as proposed by the Hammer–Nørskov model.[30] Therefore, according to the absorption population at the pre-edge regime, the upshift of the d orbital electronic states of Ag is more distinct in Ag_{AOR}–HMO than in Ag_{IMP}–HMO, which leads to stronger EMSI.[30]

The stronger EMSI in terms of the electronic states of the higher lying d orbitals were further investigated with a H_2 molecular probe, which is an effective electronic descriptor for the shifts in the electronic states of the d orbitals: the easier the reduction of the oxides at low temperature, the stronger the EMSI.[11,31,32] Thus, Ag_{AOR}–HMO has a much stronger EMSI than Ag_{IMP}–HMO judging from the temperatures (T) of the low-temperature reduction peaks (Figure 3b), which is consistent with the ΔXANES spectra.

The EMSI is a crucial factor in determining the ability of the surface to bond to a number of adsorbates, such as O_2.[32] The catalyst with the stronger EMSI is often more favorable for the activation of O_2 by increasing the DOS of its antibonding π* orbital and/or by depleting the π and 5σ bonding orbitals.[32] For silver-based catalysts, in particular, the oxidation of formaldehyde (HCHO) predominantly follows a Mars–van Krevelen mechanism,[19,33] and O_2 activation was confirmed to be one of the rate-limiting steps.[33] Consequently, Ag_{AOR}–HMO shows a higher catalytic activity than Ag_{IMP}-HMO in the oxidation of HCHO (Figure 4a; see also Figure S9) and accelerates the reaction of activated oxygen with HCHO, indicating that the nature of the CAS has a critical influence on their activities in HCHO oxidation. The CAS of Ag_{AOR}–HMO with stronger EMSI have a stronger activation ability towards O_2 than those of Ag_{IMP}–HMO, accounting for its excellent activity. The difference in nature of the CAS is apparent from the differences in activation energies (E_a), which range from 116 kJ mol^{-1} for HMO to 91 kJ mol^{-1} for the most active Ag_{AOR}–HMO, which is ascribed to the stronger EMSI (Figure 3 and Figure 4a).

To shed further light on the activation and availability of oxygen, temporal analysis of products (TAP) reactor measurements were conducted for Ag_{AOR}–HMO at two reaction temperatures using a CO probe to titrate the reactive oxygen atoms.[34] At 70 °C, there are approximately 12 (sub)surface active lattice oxygen atoms available for oxidation reactions (Figure 4b; see also Figure S10). This corresponds nicely with the number of lattice oxygen atoms that are found in the vicinity of the CAS within a radius of approximately 3.6 Å, which are accessible for oxidation reactions and can be replenished by dissociatively adsorbed oxygen at the CAS according to a structural model of Ag_{AOR}–HMO (Figure 4b, inset). At 100 °C, even more lattice oxygen atoms in the vicinity can be removed, indicating the easy reducibility of this sample and therefore a more favorable availability of the oxygen atoms for oxidation.

In conclusion, the electronic metal–support interactions of single-atom silver catalysts are controlled by the different preparation methods. The higher depletion of the d electronic state of the silver active sites results in stronger EMSI, which was demonstrated by a higher activation ability towards O_2, easier reducibility, and a higher catalytic activity in the low-temperature oxidation of formaldehyde. These results are crucial to understand the nature of intrinsic EMSI and to

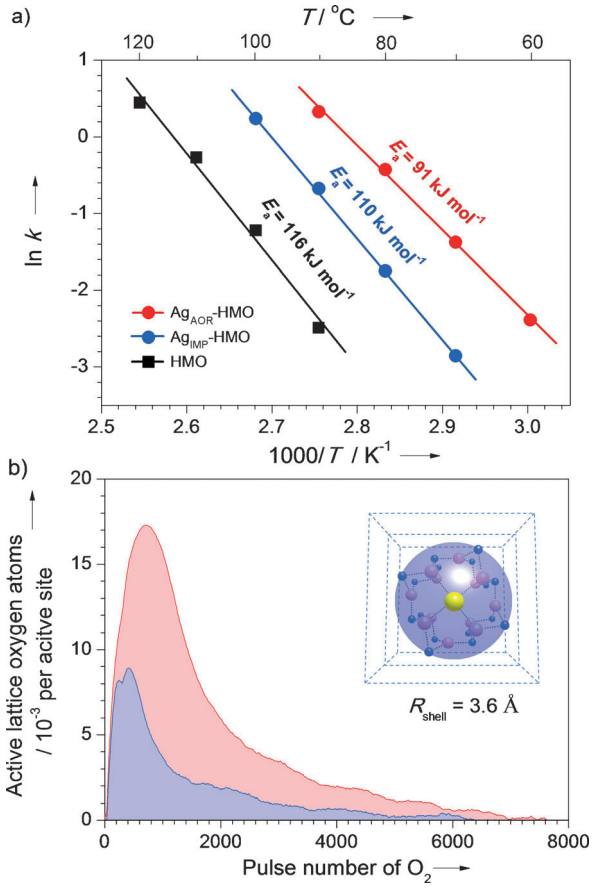

Figure 4. a) Arrhenius plots for the reaction rate constants (k) for the HCHO oxidation over the catalysts with the corresponding E_a values. b) TAP results of Ag_{AOR}–HMO at 70 °C (blue shade) and 100 °C (red and blue shades) using a CO probe. The inset model shows twelve lattice oxygen atoms (pink) within a shell with a radius of approximately 3.6 Å (R_{shell}) of the CAS (yellow) at 70 °C. Mn atoms are depicted as blue balls.

establish correlations between the electronic properties of catalytic sites and catalytic activity.

Received: October 23, 2013
Revised: January 6, 2014
Published online: March 5, 2014

Keywords: metal–support interactions · electronic structure · heterogeneous catalysis · oxygen activation · single-atom catalysis

[1] S. J. Tauster, S. C. Fung, R. L. Garten, *J. Am. Chem. Soc.* **1978**, *100*, 170–175.
[2] S. J. Tauster, S. C. Fung, R. Baker, J. A. Horsley, *Science* **1981**, *211*, 1121–1125.
[3] S. J. Tauster, *Acc. Chem. Res.* **1987**, *20*, 389–394.
[4] D. Matthey, J. G. Wang, S. Wendt, J. Matthiesen, R. Schaub, E. Lægsgaard, B. Hammer, F. Besenbacher, *Science* **2007**, *315*, 1692–1696.
[5] J. A. Farmer, C. T. Campbell, *Science* **2010**, *329*, 933–936.
[6] M. Cargnello, V. V. T. Doan-Nguyen, T. R. Gordon, R. E. Diaz, E. A. Stach, R. J. Gorte, P. Fornasiero, C. B. Murray, *Science* **2013**, *341*, 771–773.
[7] V. E. Herinch, P. A. Cox, *The Surface Science of Metal*, Cambridge University Press, Cambridge, **1996**.
[8] W. E. Kaden, T. Wu, W. A. Kunkel, S. L. Anderson, *Science* **2009**, *326*, 826–829.
[9] A. Bruix, J. A. Rodriguez, P. J. Ramírez, S. D. Senanayake, J. Evans, J. B. Park, D. Stacchiola, P. Liu, J. Hrbek, F. Illas, *J. Am. Chem. Soc.* **2012**, *134*, 8968–8974.
[10] C. T. Campbell, *Nat. Chem.* **2012**, *4*, 597–598.
[11] N. Acerbi, S. C. E. Tsang, G. Jones, S. Golunski, P. Collier, *Angew. Chem.* **2013**, *125*, 7891–7895; *Angew. Chem. Int. Ed.* **2013**, *52*, 7737–7741.
[12] M. Valden, X. Lai, D. W. Goodman, *Science* **1998**, *281*, 1647–1650.
[13] O. Lopez-Acevedo, K. A. Kacprzak, J. Akola, H. Häkkinen, *Nat. Chem.* **2010**, *2*, 329–334.
[14] W. A. De Heer, *Rev. Mod. Phys.* **1993**, *65*, 611–676.
[15] S. Dahl, A. Logadottir, R. C. Egeberg, J. H. Larsen, I. Chorkendorff, E. Törnqvist, J. K. Nørskov, *Phys. Rev. Lett.* **1999**, *83*, 1814–1817.
[16] J. K. Nørskov, T. Bligaard, B. Hvolbæk, F. Abild-Pedersen, I. Chorkendorff, C. H. Christensen, *Chem. Soc. Rev.* **2008**, *37*, 2163–2171.
[17] Y. Lei, F. Mehmood, S. Lee, J. Greeley, B. Lee, S. Seifert, R. E. Winans, J. W. Elam, R. J. Meyer, P. C. Redfern, D. Teschner, R. Schlögl, M. J. Pellin, L. A. Curtiss, S. Vajda, *Science* **2010**, *328*, 224–228.
[18] A. Uzun, V. Ortalan, N. D. Browning, B. C. Gates, *J. Catal.* **2010**, *269*, 318–328.
[19] Z. Huang, X. Gu, Q. Cao, P. Hu, J. Hao, J. Li, X. Tang, *Angew. Chem.* **2012**, *124*, 4274–4279; *Angew. Chem. Int. Ed.* **2012**, *51*, 4198–4203.
[20] A. E. Espinal, L. Zhang, C. Chen, A. Morey, Y. Nie, L. Espinal, B. O. Wells, R. Joesten, M. Aindow, S. L. Suib, *Nat. Mater.* **2010**, *9*, 54–59.
[21] C. Chen, L. Jin, A. E. Espinal, B. T. Firliet, L. Xu, M. Aindow, R. Joesten, S. L. Suib, *Small* **2010**, *6*, 988–992.
[22] F. M. Chang, M. Jansen, *Angew. Chem.* **1984**, *96*, 902—903; *Angew. Chem. Int. Ed.* **1984**, *23*, 906–907.
[23] V. Ortalan, A. Uzun, B. C. Gates, N. D. Browning, *Nat. Nanotechnol.* **2010**, *5*, 843–847.
[24] L. X. Chen, W. J. H. Jäger, G. Jennings, D. J. Gosztola, A. Munkholm, J. P. Hessler, *Science* **2001**, *292*, 262–264.
[25] C. Bressler, C. Milne, V. T. Pham, A. ElNahhas, R. M. van der Veen, W. Gawelda, S. Johnson, P. Beaud, D. Grolimund, M. Kaiser, C. N. Borca, G. Ingold, R. Abela, M. Chergui, *Science* **2009**, *323*, 489–492.
[26] S. D. George, P. Brant, E. I. Solomon, *J. Am. Chem. Soc.* **2005**, *127*, 667–674.
[27] S. G. Minasian, J. M. Keith, E. R. Batista, K. S. Boland, D. L. Clark, S. D. Conradson, S. A. Kozimor, R. L. Martin, D. E. Schwarz, D. K. Shuh, G. L. Wagner, M. P. Wilkerson, L. E. Wolfsberg, P. Yang, *J. Am. Chem. Soc.* **2012**, *134*, 5586–5597.
[28] L. H. Tjeng, M. Meinders, J. Van Elp, J. Ghijsen, G. A. Sawatzky, R. L. Johnson, *Phys. Rev. B* **1990**, *41*, 3190–3199.
[29] S. Ji, E. J. Kan, M. H. Whangbo, J. H. Kim, Y. Qiu, M. Matsuda, H. Yoshida, Z. Hiroi, M. A. Green, T. Ziman, S. H. Lee, *Phys. Rev. B* **2010**, *81*, 094421.
[30] A. Ruban, B. Hammer, P. Stoltze, H. L. Skriver, J. K. Nørskov, *J. Mol. Catal. A* **1997**, *115*, 421–429.
[31] B. Hammer, J. K. Nørskov, *Nature* **1995**, *376*, 238–240.
[32] Y. Xu, J. Greeley, M. Mavrikakis, *J. Am. Chem. Soc.* **2005**, *127*, 12823–12827.
[33] C. F. Mao, M. A. Vannice, *J. Catal.* **1995**, *154*, 230–244.
[34] D. Widmann, R. J. Behm, *Angew. Chem.* **2011**, *123*, 10424–10428; *Angew. Chem. Int. Ed.* **2011**, *50*, 10241–10245.

